Peer-reviewed version available at Entropy 2018, 20, 933; doi:10.3390/e20120933

Article

Entropy and mutability for the q-states clock model in small systems

Oscar A. Negrete [1], Patricio Vargas [1,*,2], Francisco J. Peña [1], Gonzalo Saravia[3], Eugenio E. Vogel[2,3]

[1] Departamento de Física, Universidad Técnica Federico Santa María, Valparaíso, Chile;
[2] Centro para el Desarrollo de la Nanociencia y la Nanotecnología, CEDENNA, Santiago, Chile
[3] Departamento de Ciencias Físicas, Universidad de La Frontera, Temuco, Chile.
* Correspondence: patricio.vargas@usm.cl

Academic Editor: name
Version November 13, 2018 submitted to

Abstract: In this paper, we revisit the q-states clock model for small systems. We present results for the thermodynamics of the q-states clock model from $q = 2$ to $q = 20$ for small square lattices $L \times L$, with L ranging from $L = 3$ to $L = 64$ with free-boundary conditions. Energy, specific heat, entropy and magnetization are measured. We found that the Berezinskii-Kosterlitz-Thouless (BKT)-like transition appears for $q > 5$ regardless of lattice size, while the transition at $q = 5$ is lost for $L < 10$; for $q \leq 4$ the BKT transition is never present. We report the phase diagram in terms of q showing the transition from the ferromagnetic (FM) to the paramagnetic (PM) phases at a critical temperature T_1 for small systems which turns into a transition from the FM to the BKT phase for larger systems, while a second phase transition between the BKT and the PM phases occurs at T_2. We also show that the magnetic phases are well characterized by the two dimensional (2D) distribution of the magnetization values. We make use of this opportunity to do an information theory analysis of the time series obtained from the Monte Carlo simulations. In particular, we calculate the phenomenological mutability and diversity functions. Diversity characterizes the phase transitions, but the phases are less detectable as q increases. Free boundary conditions are used to better mimic the reality of small systems (far from any thermodynamic limit). The role of size is discussed.

Keywords: q-states clock model; Entropy; Berezinskii-Kosterlitz-Thouless transition.

1. Introduction

The q-states clock model is the discrete version of the famous 2D XY model, which is probably the most extensively studied example showing the Berezinskii–Kosterlitz–Thouless (BKT) transition [1,2]. It is often used as a reference model due to its peculiar critical behaviour at the transition point and universal features [3–7]. Instead of the exclusion of an explicit continuous symmetry essential for the BKT transition, it can also emerge from a system without explicit continuous symmetry [7]. The Hamiltonian of the q-states clock model can be written in many forms, one of the simplest forms is the following expression, where no magnetic anisotropies and external magnetic field are included:

$$H = -J \sum_{i<j} \cos(\theta_i - \theta_j) \,, \tag{1}$$

where $J > 0$ is the ferromagnetic coupling connecting pairs of nearest neighbours i and j; the discrete angle between the spin orientations is given by $\theta_{i,j}(\eta, q) = 2\pi\eta/q$, for $\eta = \{0, 1, .., q-1\}$. While the exact XY model is recovered only in the limit of infinite q, it has been found that the BKT characteristics appear in the clock models when $q \geq 5$ [8–11]. The nature of the phase transitions in the general clock model has been widely studied with different theoretical and numerical approaches, which however have given mixed results for the characterization of transitions at the lower bound of q (for instance, see the summary of the related debates in [12]).

In the present work, we want to consider the clock model as a generalization of the Ising model, establishing the similarities and differences that arise due to the increase of the degrees of freedom due to the local states at each site. All of this is always aimed at the behaviour of small systems, specifically, we will focus on square lattices ranging from 3×3 up to 64×64. Free boundary conditions are preferred since they better represent the importance of surface states in small systems. The clock clock model systems under scrutiny will range from $q = 2$ (equivalent to the usual Ising model) to $q = 20$.

There are various scattered results about the thermodynamics and phase transition of the clock model. Therefore we report below a consistent compendium of its thermodynamic properties such as internal energy, U, specific heat, C, entropy S, and magnetization. We also report the transition temperatures, T_1 from the FM to the P phase for very small q values continued as the transition from the FM to the BKT phase for larger values of q, and T_2 from the BKT phase to disordered paramagnetic (P) phase. These series of results are elaborated into a phase diagram T_C vs q, where T_C is determined from the $C(T)$ curves.

The information content of a sequence was measured in what was called mutability for the first time by Vogel et al. [13] in a relationship with the characterization of the phase 2D transitions in the Edward Andersen spin system as an alternative to the Binder cumulant analysis [14]. Later on, an appropriate information recognizer was proposed (named wlzip) which optimizes recognition of digital information associated to properties of the system [15]. The method was later successfully applied to the reentrant phase diagram in the case of 3D Edwards-Anderson model. [16] Successive applications of the information content methods dealt with stock markets [17], pension funds [18], blood pressure [19], seismology [20], nematic transitions [21] and wind energy production [22].

In the present paper, we follow the approach of the magnetic transitions [13,15] complemented with the definitions of mutability and diversity [17] to be elaborated below. The aim is to have an alternative way to characterize and distinguish the phases present in the q clock model.

In the next Section, we present the clock model and the main methods used to characterize it. Presentation of results and discussion are given in Section 3, and the last Section is devoted to conclusions.

2. Model and Methods

2.1. General Definitions

Let us begin by considering the q-states clock model on a two dimensional (2D) square lattice of dimensions $L \times L = N$, where the local magnetic moment or "spin" S_i at site i can point in any of the q directions in a given plane. S_i is then a 2D vector, i.e. $S_i = (\cos(\frac{2\pi}{q}k), \sin(\frac{2\pi}{q}k))$, where $k = 0, 1, ...q-1$, with equal probability for all q values. S_i are dimensionless vectors of magnitude one.
The isotropic Hamiltonian for such a system can be written as:

$$H = -J\sum_{i>j}^{N} S_i \cdot S_j - B \cdot \sum_i S_i \,, \tag{2}$$

where $J > 0$ is the ferromagnetic exchange interaction to nearest neighbours; the sum extends to all such pairs through the lattice, which is indicated by the symbol $i > j$ under the summation symbol. B is an external field applied along one direction in the plane.
In this Hamiltonian, J is one unit of energy and B is also measured in energy units. This form is completely equivalent to the one of Equation (1), when $B = 0$.

2.2. Exact Theoretical Approach for a Small System

Let us begin by considering the theoretical approach for the q-states clock lattice with $L = 3$ introduced in the previous section. The partition function can be expressed as:

$$Z(T, B) = \sum_{n=1}^{\lambda} c_n \, e^{-E_n/T} \, , \tag{3}$$

where the coefficients c_n is the number of all of the possible spin configurations compatible with energy E_n according to the Hamiltonian of Equation (2) ; λ is the number of different energy levels. We express energy and temperature in the same units, so the Boltzmann constant is set to the unity, k_B=1. The coefficients $c_n = c(E_n, q)$ for this small $N = L \times L = 3 \times 3$ lattice can be straightforwardly calculated by using combinatorics; we show them in Table 1 for $q = 4$ and $q = 6$, and in Table 2 as examples. For all even q values (as the examples in Table 1) some symmetry rules apply: energy distribution is symmetric around $E_n = 0$, the majority of the density of states occurs for $E_n = 0$ and $c(-E_n, q) = c(E_n, q)$ holds. There are q^9 sates to be spread among all available energies in the energy range $E_n = [-12, 12]$. Due to symmetry,the total number of different energies are λ=11, 23, 47, 289 and 699 for q=2, 4, 6,8 and 10 respectively.

For odd q values the main symmetry of the Hamiltonian of Equation (2) for $B = 0$ is lost, because spin inversion $S_i \to -S_i$ is not possible . This is simply because, for odd q values, if there is S_i then $-S_i$ does not exist. Therefore the energy distribution and the corresponding degeneracy is not symmetric around $E_n = 0$. Thus, the highest possible energy is not the negative value of the ground state energy. However, as we will see, this symmetry lowering does not affect the thermodynamic observables.

Once the partition function is known, the thermodynamic observables can be calculated directly. Thus for the cases of internal energy U, specific heat C, and entropy S, they can be obtained employing:

$$U(T) = T^2 \frac{\partial}{\partial T} \ln Z(T, B) \, , \tag{4}$$

$$C(T) = \frac{\partial U}{\partial T} \, , \tag{5}$$

$$S(T) = \frac{U}{T} + \ln Z(T, B) \, . \tag{6}$$

Table 1. Coefficients $c(E_n, q)$ for a 3×3 lattice with free boundary conditions and B=0, for $q = 4$ and $q = 6$. The first column enumerates energy levels, n, second and third columns give the corresponding energies E and degeneracies $c(E, 4)$ respectively. Fourth and five columns show half of energies and degeneracies for $q = 6$ respectively. The rest of the energies and degeneracies can be found using the following symmetry: $c(-E_n, 6) = c(E_n, 6)$.

	q = 4		**q = 6**	
n	E_n	$c(E_n, 4)$	E_n	$c(E_n, 6)$
1	-12	4	-12	6
2	-10	32	-11	48
3	-9	128	-10.5	192
4	-8	248	-10	348
5	-7	896	-9.5	960
6	-6	2336	-9	2448
7	-5	4864	-8.5	2736
8	-4	10748	-8	5376
9	-3	19712	-7.5	11808
10	-2	29376	-7	14880
11	-1	39936	-6.5	22128
12	0	45584	-6	54072
13	1	39936	-5.5	54960
14	2	29376	-5	94032
15	3	19712	-4.5	175968
16	4	10748	-4	191514
17	5	4864	-3.5	231744
18	6	2336	-3	478752
19	7	896	-2.5	393360
20	8	248	-2	530892
21	9	128	-1.5	806736
22	10	32	-1	707760
23	12	4	-0.5	701712
24			0	1112830

Next table shows the results for $q = 5$ where the energies E_n and degeneracies for $n = 1$ to $n = 85$ are explicitly given. In this case for a given energy E_n, their negative counterpart does not exists.

Table 2. Coefficients $c(E_n,5)$ for a 3×3 lattice with free boundary conditions and B=0. In this case there are no symmetries and therefore we present all E_n values with their respective degenerations, from $n = 1$ to $n = 85$. Here, as explained in the manuscript the symmetry $S_i \to -S_i$ is not present.

q = 5											
n	E_n	$c(E_n,5)$	n	E_n	$c(E_n,5)$	n	E_n	$c(E_n,5)$	n	E_n	$c(E_n,5)$
1	-12	5	23	-4.92705	15760	45	-1.57295	15760	67	2.30902	89000
2	-10.618	40	24	-4.76393	290	46	-1.47214	4100	68	2.47214	1340
3	-9.92705	160	25	-4.66312	6720	47	-1.30902	124320	69	2.73607	58080
4	-9.23607	290	26	-4.5	8960	48	-1.1459	1680	70	3	30200
5	-8.54508	800	27	-4.23607	30360	49	-1.04508	27920	71	3.16312	6720
6	-8.38197	40	28	-4.07295	680	50	-0.881966	57000	72	3.42705	64120
7	-8.11803	320	29	-3.97214	5280	51	-0.618034	117040	73	3.8541	21160
8	-7.8541	1680	30	-3.80902	23080	52	-0.454915	6958	74	4.11803	23640
9	-7.42705	680	31	-3.7082	410	53	-0.354102	9200	75	4.28115	1440
10	-7.16312	1600	32	-3.54508	29120	54	-0.190983	124320	76	4.54508	27920
11	-7	39936	33	-3.38197	5800	55	0	2	77	4.97214	5280
12	-6.73607	3040	34	-3.28115	1680	56	0.072949	64120	78	5.23607	17720
13	-6.57295	160	35	-3.11803	57000	57	0.236068	30360	79	5.66312	9880
14	-6.47214	1340	36	-2.95492	800	58	0.5	147600	80	6.09017	560
15	-6.30902	1760	37	-2.8541	21160	59	0.663119	1600	81	6.3541	9200
16	-6.04508	6960	38	-2.69098	23080	60	0.763932	17720	82	6.78115	1680
17	-5.88197	320	39	-2.59017	1240	61	0.927051	77360	83	7.47214	4100
18	-5.78115	1440	40	-2.42705	77360	62	1.19098	89000	84	8.59017	1240
19	-5.61803	5800	41	-2.26393	3040	63	1.3541	8440	85	9.70820	410
20	-5.3541	8440	42	-2.16312	9880	64	1.61803	117040			
21	-5.19098	1760	43	-2	67600	65	1.88197	23640			
22	-5.09017	560	44	-1.73607	58080	66	2.04508	29120			

We invoke now the numeric simulations to calculate larger sizes for the same system.

2.3. Numerical Simulations

In addition to the theoretical calculations, most of the work will deal with numerical calculations based on Monte Carlo (MC) simulations. A square lattice $L \times L$ is chosen; free boundary conditions are imposed; a site is randomly visited, and the energy cost, Δ, of rotating the corresponding spin around q possible states is calculated: if the energy is lowered, the change of orientation is accepted; otherwise, only when $\exp(-\Delta/T) \leq r$, the spin rotation is accepted, where r is a freshly-generated random number in the range [0,1] with equal probability. This is the usual Metropolis algorithm. A Monte Carlo step (MCS) is reached after $N = L \times L$ spin-rotation attempts. One of the main goals here is to report the sensitive temperatures T_1 and T_2 defining the transition from FM to BKT and from BKT to PM (disordered) phase, for different systems.

For each lattice size and q value a sequence of temperatures was defined in the range [0.02,3] at steps of 0.02 for each temperature, 5τ MCSs are performed: the first τ MCS is used to equilibrate at a fixed temperature T, while the next 4τ MCS is used to measure the observables every 20 MCSs, reaching a total of $2 \times 10^5 = 200,000$ measurements. Unless specified in a different way $\tau = 10^6$ in the rest of the paper; this τ value gives stable results and leads to coincidence with the analytic expressions obtained as described above. The energy $U(T)$ is computed according to the Hamiltonian given by Equation (2). With the internal energy known as a function of T Equations (4), (5) and (6) can be used to generate the thermodynamics. In parallel, the magnetization $M(T)$ for each temperature can also be instantaneously measured. Alternatively, we can also use direct relationships based on the thermal treatment of the variables as presented next.

Peer-reviewed version available at Entropy 2018, 20, 933; doi:10.3390/e20120933

2.4. Thermal averages

The lattice average of the spin configuration, equivalent to the magnetization per site M, is given by the following expression:

$$M = \frac{1}{N}\sum_{j=1}^{N} S_j \,, \tag{7}$$

where S_j is the value of the spin at site j at a given time, t, and $N = L \times L$, is the total number of spins. In this particular case M is a vector of two components $M = (M_x, M_y)$. Normally, the magnitude or absolute value of this vector is calculated, i.e. $|M| = \sqrt{M_x^2 + M_y^2}$. Then, the thermal average of the absolute value $|M|$, is $< |M| >$ and it is given by

$$< |M| >= \frac{1}{N_c}\sum_{i=1}^{N_c} \sqrt{M_x^2 + M_y^2} \,, \tag{8}$$

where $N_c = 2 \times 10^5$ is the number of configurations used to perform thermal averages, as explained in the preceding section.
Energy is the main quantity used in the Monte Carlo method to reach thermal equilibrium. Therefore, after τ MCSs the internal energy U can be obtained by averaging the $N_c = 2$ values for E_k, where k runs over the accepted configurations after the Metropolis algorithm, namely:

$$U =< E >= \frac{1}{N_c}\sum_{k=1}^{N_c} E_k \,, \tag{9}$$

where every spin configuration is separated from the next one by 20MCs. The energy per site is then, U/N, which is the thermal average of the lattice average of the system energy.
The specific heat is then calculated as proportional to the fluctuations of the energy as follows:

$$C = \frac{\langle E^2 \rangle - \langle E \rangle^2}{T^2} \,, \tag{10}$$

$$C = \frac{1}{T^2}\left[\left(\frac{1}{N_c}\sum_{k=1}^{N_c} E_k^2\right) - \left(\frac{1}{N_c}\sum_{k=1}^{N_c} E_k\right)^2\right] \,. \tag{11}$$

The absolute entropy S can be calculated by calculating $\Delta S(T_f, T_i) = S(T_f) - S(T_i)$ by numerical integration of the specific heat divided by the temperature, as follows:

$$\Delta S(T_f, T_i) = \int_{T_i}^{T_f} \frac{C(T)}{T} dT \,. \tag{12}$$

We know the entropy at zero temperature, because we know the energy degeneration at $T = 0$. For the case $B \neq 0$, only one spin configuration has minimum energy (every spin aligned to B), therefore $S(0) = 0$. On the other hand, when the magnetic field is zero, there are q ferromagnetic spin configurations with equal energies. Therefore, $S(0) = \ln q$, hence then $S(T) = \ln q + \Delta S(T, 0)$.

As we have seen, the thermal average of a physical quantity, is a summation over N_c quantities (normalized to N_c), like the energies, magnetic moments, etc. However, the order of the sequence of these N_c quantities is totally irrelevant in the result of this evaluation. Next we introduce the mutability which is a quantity (defined in terms of information theory) that can be calculated from any temporal sequence of quantities, like the energy, magnetic moment, etc. Mutability is a quantity that depends on the sequence order, and therefore contains different information than a mere average.

2.5. Information theory, mutability and diversity

Word length zipper (wlzip for short) is a compressor designed to recognize meaningful information in a data chain. As its name tells it recognizes "words" of precise length and precise location within the data chain. Then, it compresses less than other file compressors which precisely optimize this function. In the case of wlzip the optimization is on the recognition of patterns beginning at a precise location and for a given number of digits. In this way, physical properties and/or other inherent properties of the system can be recognized.

The recognition of information within a file can render at least two parameters: mutability and diversity. They were defined a few years ago including a working example given in Table 2 of Ref. [15] Here we will very briefly review these definitions beginning with the basic rules under which wlzip operates. Let us assume our data is contained in a vector file (one register per row) named "data.txt" whose number of rows is $\lambda(data)$ and its weight in bytes is $w(data)$. We now create a map of previous file in the following way: we go over each row of data.txt and whenever this value is new we add it as a new row to a new file which will me named map.txt. So the process begins with the first element of data.txt which is also the first element in map.txt. Then the second element of data.txt is considered: if this element is new we add it as a second row in map.txt; if this element is the same as the previous one one we just add a digit 1 to the right of this element in map.txt (1 here means one position from last time this element appeared). The process continues like that so each time a new record is detected a new row in map.txt is created, while repetitions are indicated as progressions of relative positions to the right of the register in map.txt. At the end of the process, map.txt contains as many rows as different values were present in data.txt; the more a value is repeated the wider the corresponding row is in map.txt. In a sense this is like a histogram organized according to the appearance order. The number of rows in data.txt is $\lambda^*(map)$, while the weight of this file is $w^*(map)$.

The mutability $\mu(data)$ of the entire file data.txt is simply given by

$$\mu(data) = \frac{w^*(data)}{w(data)}. \tag{13}$$

Similarly, the diversity of the file data.txt is also a ratio, namely

$$\delta(data) = \frac{\lambda^*(data)}{\lambda(data)}. \tag{14}$$

Previous definitions can be also dynamic at the time t and considering the ν records in data.txt counted from that one at time t. Then we can define the dynamic parameters associated to data.txt:

$$\mu(t,\nu) = \frac{w^*(t,\nu)}{w(t,\nu)} \tag{15}$$

and

$$\delta(t,\nu) = \frac{\lambda^*(t,\nu)}{\lambda(t,\nu)}. \tag{16}$$

As it was shown in the discussion accompanying Figure 1 of Ref. [17] referred to the Ising model, mutability can be more appropriate to discuss variability of a parameter with changing conditions (like increase of temperature) while diversity is more appropriate to discuss critical phenomena such as phase transitions. This is one of the issues to be discussed below under the light of the results obtained from the clock model.

3. Results and Discussions

Let us begin by considering the theoretical approach for the q-states clock model following Equation (2) for $B = 0$, considering a $L = 3$ lattice as it was presented in the previous section. We have successfully calculated the partition functions from $q = 2$ (Ising) to $q = 10$. From here, all the

thermodynamic quantities of the system can be analytically obtained as a function of the temperature T.
Figure 1 shows the results obtained for internal energy $U(T)$, specific heat $C(T)$, and entropy $S(T)$.

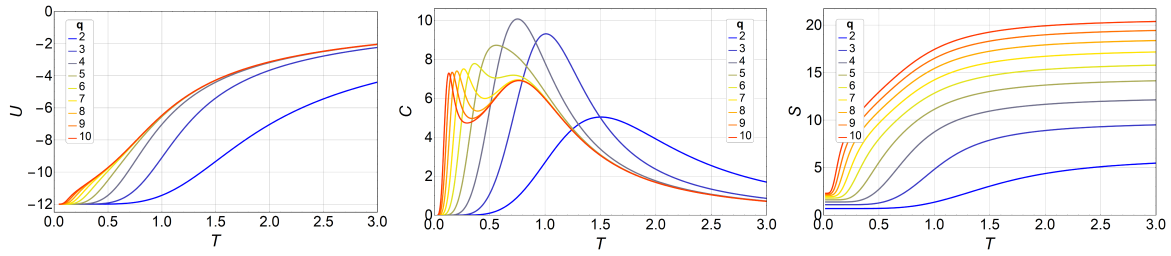

Figure 1. Internal Energy, U (left), Specific heat, C (middle), and Entropy, S (right), of the q-states clock model as a function of temperature, T for a 3×3 lattice, without magnetic field, for different values of q. From $q = 2$ (blue) to $q = 10$ (red).

In the case of the specific heat, C vs T (center of Figure 1) we see that the two peaks appear for $q \geq 6$. At $q = 5$ we see only one peak, but notoriously more skewed to the right. We will see that this is due to the small size of the lattice. Therefore for small systems, the BKT phase appears only for $q \geq 6$. We can see here (Figure 1 right) the basic features of entropy in the low and high-temperature limits. When no external field is applied, the energy ground state of the ferromagnetic q-states clock model has a degeneracy equal to q, independent of the total number of spins N, therefore $S(0) = \ln q$. On the other hand, at very high temperatures, the exchange interaction is overridden, and every spin has q degrees of freedom with equal probabilities, hence the system degeneracy is equal to q^N, and therefore the entropy $S(T >> J) = N \ln q$, which is what it is observed in Figure 2.
Figure 2 shows the same observables in the presence of magnetic field B, namely, $U(T, B)$, $C(T, B)$ and $S(T, B)$ for the case $q = 7$ as an example; the shift of the transition temperatures due to the variations of the magnetic field is clearly appreciated. This is also an exact analytical result obtained by calculating straightforwardly the partition function of Equation (3). The magnetic field was applied along the (1,0) direction, along which a possible spin orientation is always possible regardless of the q value.

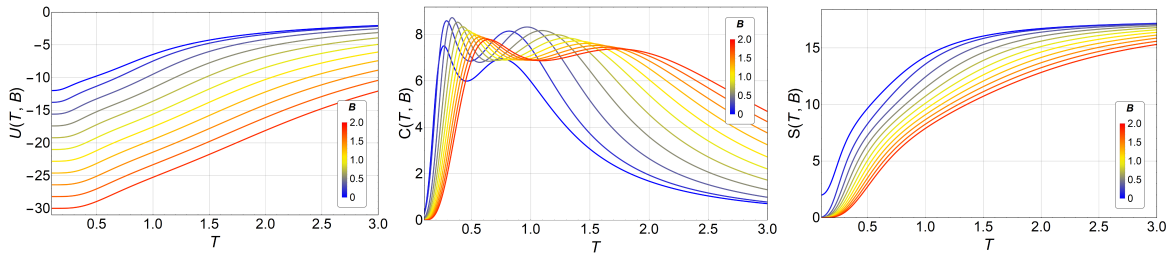

Figure 2. Internal Energy, $U(T, B)$ (left), Specific heat, $C(T, B)$ (middle), and Entropy, $S(T, B)$ (right), of the q-states clock model ($q = 7$) as a function of temperature, T and field, B, for a 3×3 lattice. Different magnetic fields, B, are indicated by lines of different colors, from $B = 0$ (blue) to $B = 2$(red).

For $B > 0$ the Zeeman term is added to the energy (see Equation (2)); therefore the FM ground state energy is lowered by the external field. As an example for $B = 2$, the Zeeman energy is -18, and this is added to the ground state energy (-12) at zero field; therefore the new ground state energy is -30 (red curve in the left of Figure 2.
We also observe that the specific heat, C vs T shapes maintain the two peaks, but they shift to higher temperatures as the external field goes from $B = 0$ to $B = 2$. This behavior is easily explained because

the external field favours ordered phases (FM and BKT) against disorder, and therefore the transition temperatures increase with the strength of the external field.
The magnetic field breaks ergodicity, therefore at $T = 0$ there is only one ground state, thus $S = 0$ for $B \neq 0$. However, at high temperatures the Zeeman term in Equation (2) is overridden and we are back to the same situation as in previous analysis for $B = 0$, namely, every spin has q degrees of freedom with equal probabilities, hence the system degeneracy is equal to q^N, and therefore the entropy $S(T >> J) = N \ln q$, which is what it is observed in the right of Figure 2.

3.1. MonteCarlo simulations

Next, we present and discuss the output from Monte Carlo simulations made for the q-states clock model in lattices up to 64×64, with free boundary conditions. We began by simulating a 3×3 lattice for different q values and comparing this numerical results to the analytic ones presented in the previous section. We did not find a single difference, which is expected of course, but which also serves as a check for the computer programs used extensively in the simulations reported next. Thus, thermodynamic observables for lattices 10×10, 16×16, 32×32 and 64×64, are presented in figures 3 through 6 respectively.

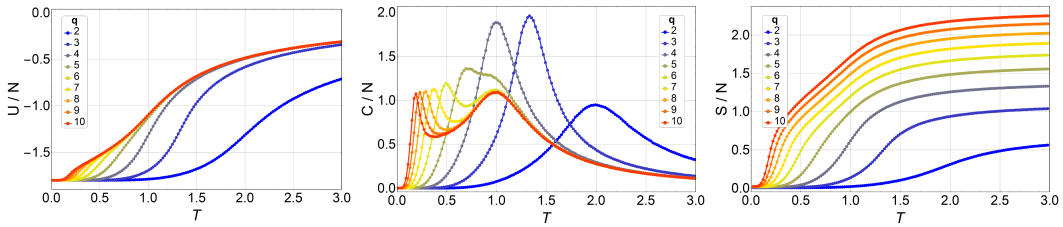

Figure 3. Internal Energy, U/N (left), Specific Heat C/N (middle) and Entropy S/N (right) of the q-states clock model as a function of temperature, T for a $N = 10 \times 10$ lattice, without magnetic field, for $q = 2$ (blue) to $q = 10$ (red).

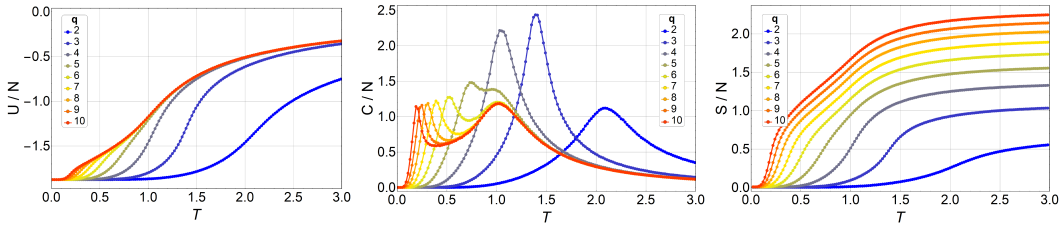

Figure 4. Internal Energy, U/N (left), Specific Heat C/N (middle) and Entropy S/N (right) of the q-states clock model as a function of temperature, T for a $N = 16 \times 16$ lattice, without magnetic field, for $q = 2$ (blue) to $q = 10$ (red).

Preprints (www.preprints.org) | NOT PEER-REVIEWED | Posted: 13 November 2018 doi:10.20944/preprints201811.0296.v1

Peer-reviewed version available at Entropy 2018, 20, 933; doi:10.3390/e20120933

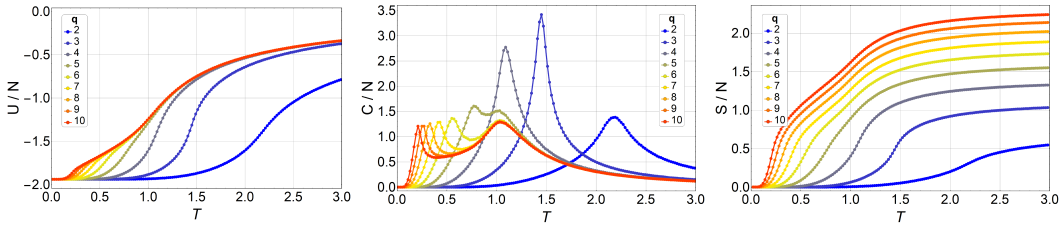

Figure 5. Internal Energy, U/N (left), Specific Heat C/N (middle) and Entropy S/N (right) of the q-states clock model as a function of temperature, T for a $N = 32 \times 32$ lattice, without magnetic field, for $q = 2$ (blue) to $q = 10$ (red).

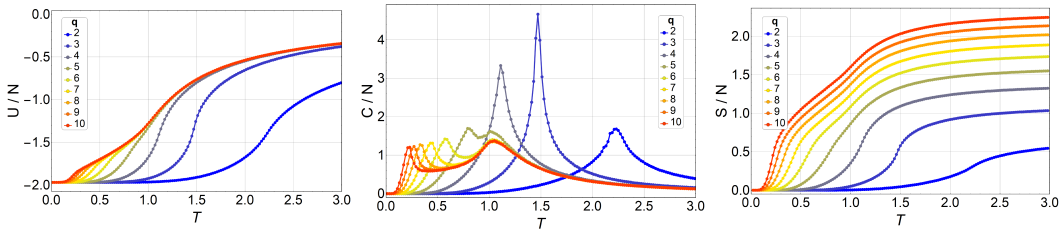

Figure 6. Internal Energy, U/N (left), Specific Heat C/N (middle) and Entropy S/N (right) of the q-states clock model as a function of temperature, T for a $N = 64 \times 64$ lattice, without magnetic field, for $q = 2$ (blue) to $q = 10$ (red).

We observe an overall self-agreement in the shape of the Energy U, Specific Heat C, and Entropy S, as functions of temperature for the different lattices. The most noticeable change is the decrease in temperature for the low-temperature peak in the specific heat curve as the size of the lattice increases. For a given size, the peak of the specific heat occurs at a lower temperature as q increases, and then it splits in two peaks. As q continues to increase, the high-temperature peak remains at the same temperature whereas the low-temperature peak tends to lower temperatures (eventually to zero temperature) as q increases tending to infinity. This low-temperature peak, T_1, is the transition from the FM phase to the BKT like phase, which is characterized by vortex spin configurations and FM spin-spin correlated configurations like waves. Both, vortex and spin waves are low energy excitation that occurs as q increases, therefore in the $q \to \infty$ we expect that $T_1 \to 0$. To be more specific about the characterization of the clock model, we discuss next a phase diagram including the three possible magnetic phases: FM (long-range order), BKT (short-range correlations) and PM (total disorder).

3.2. Phase diagram

In this section, we show the phase diagram for the clock model as extracted from the specific heat. We collected the analytic results for the 3×3 lattice and the numerical results for the 10×10 and the 64×64 lattices. This is shown in Figure 7 for q ranging from 2 to 20 by means of squares, triangles and circles respectively. The texture and colour underneath illustrate the instantaneous magnetic phases for the larger lattice and $q = 9$ just as examples for the kind of magnetic ordering present in each phase.

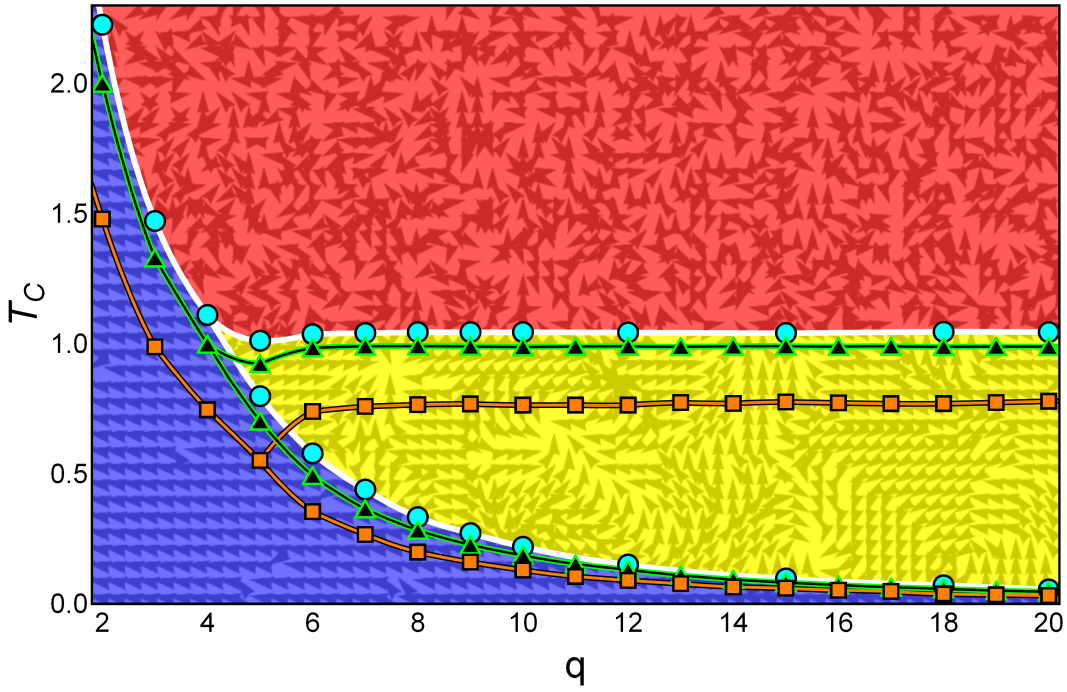

Figure 7. Phase diagram for the q-states clock model for a 3×3 lattice (squares), a 10×10 lattice (triangles) and a 64×64 lattice (circles) with free boundary conditions. For temperatures under T_1 the FM ordered phase dominates. For $q < 5$ the transition from this phase is to the disordered PM phase. For large enough lattices and $q \geq 5$ the transition from the FM phase is to the partially ordered BKT phase. Then, a transition at a higher temperature T_2 appears separating the BKT phase from the PM phase; it can be noticed that T_2 is essentially constant with respect to q. Background colors blue, yellow and red (from bottom to top) mark the FM, BKT and PM phases respectively. Spin orientations for one possible snapshot corresponding to the 64×64 lattice and $q = 9$ are given in gray color over the background colors.

Several features in Figure 7 deserve special discussion. First, the lower critical temperature T_1 follows a monotonous decrease with q approaching zero asymptotically. Second, the higher critical temperature T_2 keeps a constant value for $q \geq 6$. Third, for $q = 5$ there is just one critical temperature following the tendency of T_1, but for $q = 10$ (and also for $q = 64$) the two transitions are clearly appreciated for $q = 5$. Fourth, an order parameter beyond the usual magnetization is necessary to distinguish the BKT phase from the PM disordered phase.

To be more specific about the different phases, Figure 8 shows the specific heat for a 32×32 lattice as a function of temperature, where we show a two-dimensional (2D) order parameter, at certain characteristic temperatures, which clearly discriminate the three (FM, BKT and PM) different phases. The order parameter we use is the 2D distribution of the variable $M = (M_x^c, M_y^c)$, as defined in Eq. (7) , the spin-lattice average at time t after the thermalization process of τMCSs.
This corresponds to the vector spin average for a given spin configuration at time, t. This vector is then calculated after the thermalization, and every 20MCSs in a total of N_c times. By plotting all N_c vectors, we generate a 2D distribution that clearly characterizes the different phases. In the FM phase, only certain directions of the spin are allowed, in the Figure 8 made for $q = 9$ we see at low temperature, that average magnetization vector points in nine directions which correspond to the nine-fold symmetry of the FM states with equal probability. The BKT like phase is characterized by spin waves and vortex structures; therefore the lattice average of the spin points to any of the 2π directions but conserving in great extent its magnitude in every lattice average. Therefore a ring structure is formed. In the disordered (PM) phase every spin in the lattice points randomly to any direction; therefore the lattice average magnetization distribution exhibits a 2D-gaussian peak with

Preprints (www.preprints.org) | NOT PEER-REVIEWED | Posted: 13 November 2018 doi:10.20944/preprints201811.0296.v1

Peer-reviewed version available at Entropy 2018, 20, 933; doi:10.3390/e20120933

decreasing magnitude as T increases; hence the circle begin to be filled with a higher probability (red color) near the center. The color code goes from black (zero value), purple, blue, green, yellow and red in increasing order of probability for this 2D order parameter. This parameter was already introduced as a complex order parameter by Baek et al. [24]

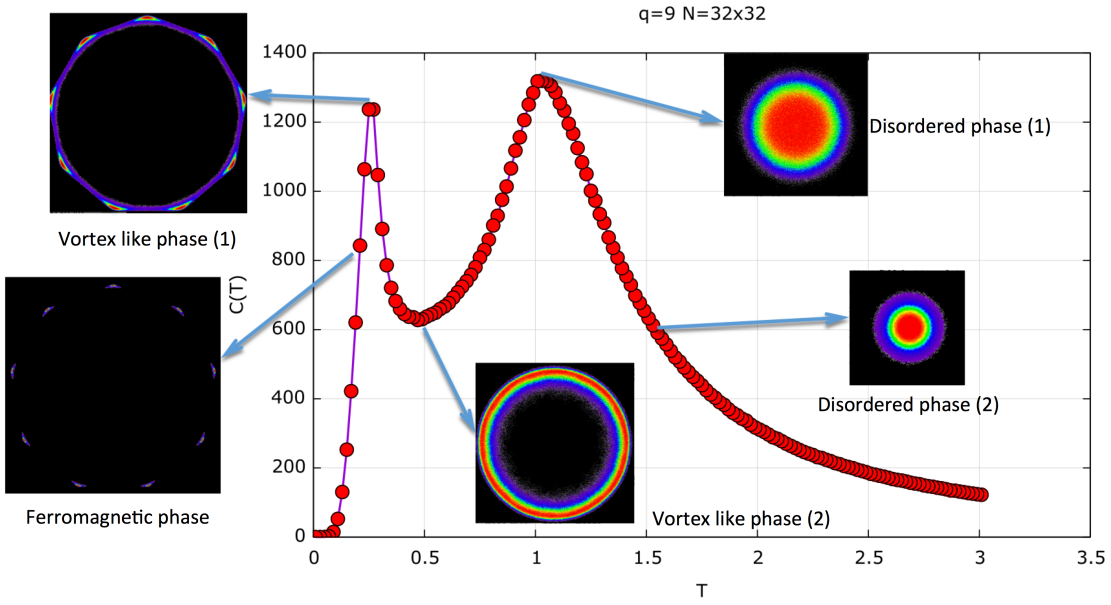

Figure 8. Specific heat for $q = 9$ in a 32×32 lattice (red curve). The figures depict the 2D order parameter distribution of M (two component vector), as defined in the text, for $T = 0.21, 0.27, 0.5, 1$ and 1.51. In the ferromagnetic (FM) phase the distribution presents a nine-fold symmetry, indicating the 9 possible orientations of the magnetic domains in the FM phase at T=0.21. Vortex-like phase (1) shows ($T = 0.27$) the onset of the BKT phase where we have smaller FM domains and vortex structures. This makes the thermal average magnetization (the 2D order parameter) to rotate but keeping its overall magnitude, at T=0.27 there is a reminiscence of the FM phase still present as can be seen in the ring structure with 9 maxima as observed at $T = 0.21$. In T=0.5 a pure BKT phase is observed as a uniform ring structure but their radius begin to shrink, maintaining a smaller magnitude. At $T = 1$ is the onset of the disordered phase in which the magnitude of the magnetization decreases, filling the interior of the circle as a 2D Gaussian distribution with zero average, at $T = 1.51$, the overall magnitude of the M parameter further shrinks. The color code of the 2D order parameter distribution goes from black, purple, blue, green, yellow and red as values of the 2D distribution increase. The radii of the ring-like 2D distributions represent the thermal magnetization modulus as a function of temperature, and this is given in Figure (10).

Next figure depicts snapshots of some spin configurations showing the spin arrangements that occur different temperatures.

Preprints (www.preprints.org) | NOT PEER-REVIEWED | Posted: 13 November 2018 doi:10.20944/preprints201811.0296.v1

Peer-reviewed version available at Entropy 2018, 20, 933; doi:10.3390/e20120933

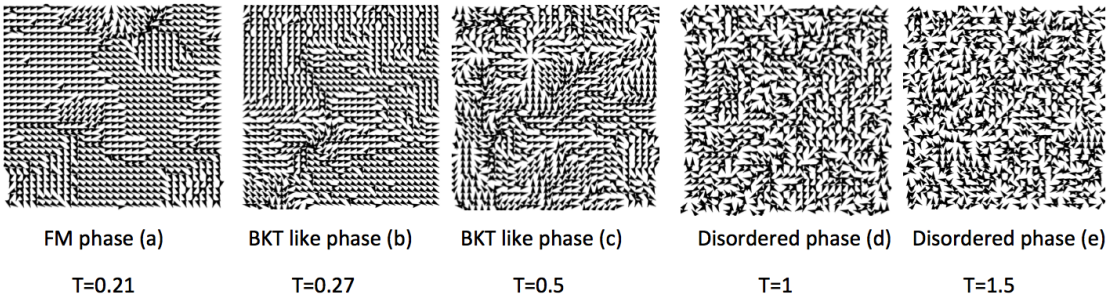

.

Figure 9. Spin arrangements of the q-states clock model for $q = 9$ in a 32×32 lattice. The figure depicts five snapshots each of one as a sample out of the 2×10^5 states used for thermal averages, at different temperatures. The temperatures are the same as shown in Figure 8, i.e. $T = 0.21, 0.27, 0.5, 1$ and 1.51. The snapshots clearly show the FM phase (a), the BKT like phase (b) and (c), and the disordered phase (d) and (e).

Next figure shows the magnetization modulus as the thermal average of the spin-lattice average, as defined in Eq. (8)

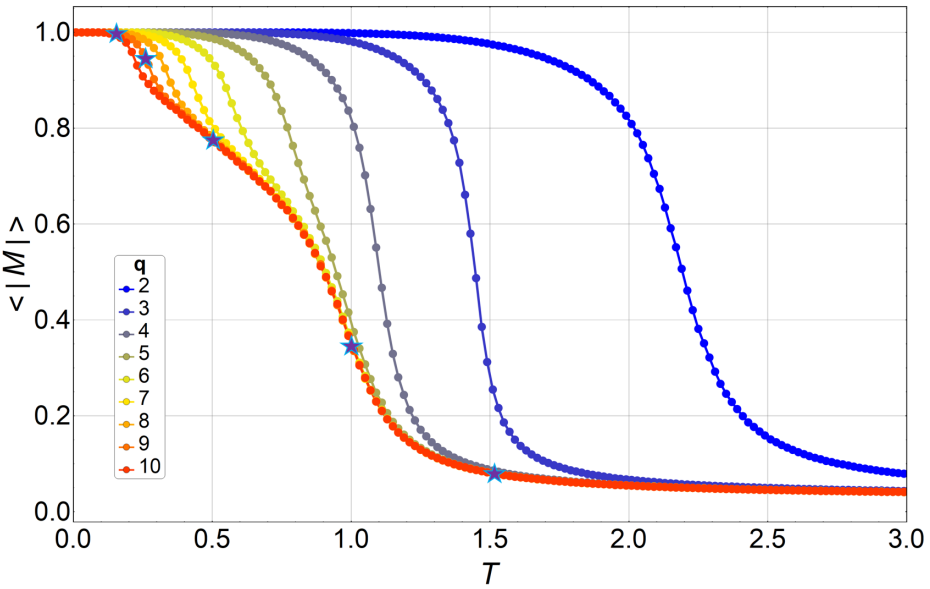

Figure 10. Thermal average of the absolute value of the magnetization, as defined in Eq.(8) (for $q = 2$ (blue) to $q = 10$(red) in a 32×32 lattice. The figure also depicts five starts for $q = 9$ at the temperatures where the 2D order parameter are shown in Figure 8, for $T = 0.21, 0.27, 0.5, 1$ and 1.51. The values of their absolute magnetizations are the average radii of the ring and circular point distributions shown in Figure 8.

Let us now consider the information content as an independent test to characterize these phase transitions. We shall concentrate on the simulations for lattices 32×32 measuring μ and δ as defined in the Methodology Section.

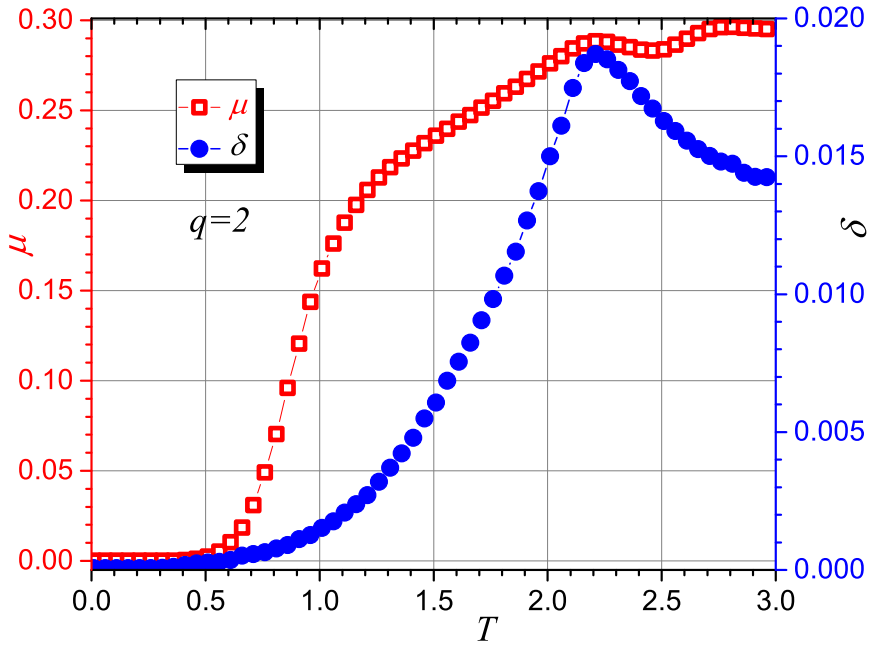

Figure 11. Mutability (μ) and diversity (δ) associated to the energy data for $L = 32$, $q = 2$.

Figure 11 presents the information content results for the same energy series generated by the previously described MC algorithm; the case of a 32×32 lattice for $q = 2$ is chosen for this report. The open squares curve (red) gives the results for mutability, which presents a local maximum near $T = 2.2$ in agreement with the specific heat results (see Figure 5). The solid circle's curve (blue) is the result for diversity showing a sharper absolute maximum at $T = 2.2$. These are the results obtained from the energy data; however, there are better parameters to register magnetic ordering whose consideration is beyond the goals of the present paper [17]. At the moment we will stick to the energy data results treated with diversity to directly compare with the energy curves, entropy and specific heat results reported above.

In Figure 12 we present the results for δ in the cases for $q = 3$, $q = 4$, $q = 6$ and $q = 8$. The ordinates have been multiplied by appropriate constants to fit in a common arbitrary scale since the meaningful information is in the temperatures that are marked by each maximum or the inflections of the curves. For $q = 3$ just one critical temperature is appreciated in agreement with the maximum of the specific heat for this lattice size as shown in Figure 5. A similar situation is observed for $q = 4$ maximizing at lower temperatures around 1.1. For $q = 6$ a maximum around 1.1 and a "knee" just over 0.5 are visible in agreement with the two maxima for this value of q reported in the figure for specific heat. In the case of $q = 8$, the maximum near 1.1 is clearly present although a bit broader than for $q = 6$. The "knee" is barely appreciated as a tiny change of slope under $T = 0.5$.

The results shown by previous two figures and similar ones for other intermediate values of q show that the information method is able to recognize the transitions present in the clock model for low values of q when this is applied to the energy data vectors produced by the MC simulations. However, the phases are less detectable by this method as q increases. Eventually, a different order parameter more oriented to the magnetic states of the system rather than just the energy levels could render better results. At the moment this is an open question, and it should be addressed in future work.

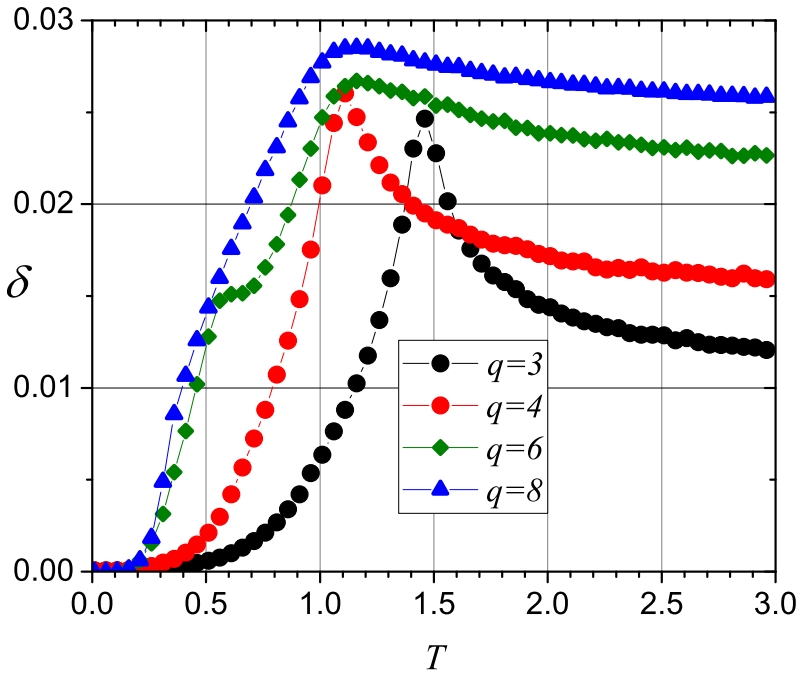

.

Figure 12. Diversity δ associated to the energy data for $L = 32$, $q = 3$, $q = 4$, $q = 6$ and $q = 8$

4. Conclusions

Using analytically derived expressions and Monte Carlo simulations we explored the q-states clock model for square lattices with free boundary conditions which better mimic the properties of small systems to which this approach is intended. We calculated their thermodynamic properties and characterized the three magnetic phases present for this model. The corresponding magnetic phase diagram was calculated for lattices sizes up to 64×64. It turns out that there exists a FM below a critical temperature T_1. For $q \geq 5$ and lattice sizes over 10×10 a BKT-like phase appears for temperatures between T_1 and a second critical temperature T_2 separating this BKT phase from the disordered paramagnetic phase. The BKT phase reflects partial magnetic ordering characterized by vortex spin configurations and zones with FM spin-spin correlation, reflecting curling or wave-like ordering. The three phases can be well characterized using the lattice spin average distribution. This 2D distribution shows characteristic patterns which clearly identify the three (FM, BKT and PM) phases.

The entropy of the system always increases with temperature showing subtle slope changes at the transition temperatures T_1 and T_2. The low-temperature limit for the entropy is simply given by $\ln(q)$ in absence of magnetic field while it vanishes for any magnetic field that breaks ergodicity yielding a singlet as a ground state. On the other hand, the high-temperature value for entropy tends asymptotically to $N \ln(q)$ thus reflecting that all degrees of freedom are equally probable.

The information theory method produces results in agreement with those of the specific heat of the system. It distinguishes the phase diagram presented in Figure 7 for low values of q thus confirming previous results obtained by conventional treatments. However, this recognition is progressively lost as q increases. This is probably due to the fact that the information recognition pointed to the energy values which are shared by more and more states as q increases (contribution of the internal degrees of freedom to the density of states). Eventually, different simulations involving a more elaborated order parameter is needed to cope with the slight difference between the BKT phase and the disorder phase,

both with vanishing magnetization. This work is in progress and should produce results in the near future.

Acknowledgments: Francisco J. Peña acknowledges the financial support of FONDECYT-postdoctoral 3170010. P. Vargas and E. Vogel acknowledge support from Financiamiento Basal para Centros Científicos y Tecnológicos de Excelencia, under Project No. FB 0807 (Chile), P. Vargas acknowledges USM-DGIIP grant number PI-M-17-3 (Chile). E. Vogel acknowledges partial support from Fondecyt 1150019.

Author Contributions: P. Vargas and E. Vogel conceived the idea and formulated the theory. O. Negrete built the computer program and edited the figures. G. Saravia wrote the mutability code. P. Vargas write the first version of the manuscript, Francisco J. Peña contributed with discussions in the writing and edition of the same. All authors have read and approved the final manuscript.

Conflicts of Interest: The authors declare no conflict of interest.

References

1. Berezinskii, V.L. Destruction of Long-range Order in One-dimensional and Two-dimensional Systems having a Continuous Symmetry Group I. Classical Systems. *Zh. Eksp. Teor. Fiz.* **1971**, *59*, 907–920.
2. Kosterlitz, J.M.; Thouless, D.J. Long range order and metastability in two dimensional solids and superfluids. (Application of dislocation theory). *J. Phys. C Solid State Phys.* **1972**, *5*, L124.
3. Kosterlitz, J.M.; Thouless, D.J. Ordering, metastability and phase transitions in two-dimensional systems. *J. Phys. C Solid State Phys.* **1973**, *6*, 1181–1203.
4. Kosterlitz, J.M. The critical properties of the two-dimensional xy model. *J. Phys. C Solid State Phys.* **1974**, *7*, 1046–1060.
5. Jose, J.V.; Kadanoff, L.P.; Kirkpatrick, S.; Nelson, D.R. Renormalization, vortices, and symmetry-breaking perturbations in the two-dimensional planar model. *Phys. Rev. B* **1977**, *16*, 1217–1241.
6. Kenna, R. The XY Model and the Berezinskii-Kosterlitz-Thouless Phase Transition. *arXiv* **2005**, arXiv:cond-mat/0512356.
7. *40 Years of Berezinskii-Kosterlitz-Thouless Theory*; Jose, J.V., Ed; World Scientific: London, UK, 2013.
8. Elitzur, S.; Pearson, R.B.; Shigemitsu, J. Phase structure of discrete Abelian spin and gauge systems. *Phys. Rev. D* **1979**, *19*, 3698–3714.
9. Cardy, J.L. General discrete planar models in two dimensions: Duality properties and phase diagrams. *J. Phys. A Math. Gen.* **1980**, *13*, 1507–1515.
10. Fröhlich, J.; Spencer, T. The Kosterlitz-Thouless transition in two-dimensional Abelian spin systems and the Coulomb gas. *Commun. Math. Phys.* **1981**, *81*, 527–602.
11. Ortiz, G.; Cobanera, E.; Nussinov, Z. Dualities and the phase diagram of the p-clock model. *Nucl. Phys. B* **2012**, *854*, 780–814.
12. Borisenko, O.; Cortese, G.; Fiore, R.; Gravina, M.; Papa, A. Numerical study of the phase transitions in the two-dimensional Z(5) vector model. *Phys. Rev. E* **2011**, *83*, 041120.
13. Vogel, E.E.; Saravia, G.; Bachmann, F.; Fierro, B.; Fischer, J. Phase transitions in Edwards-Anderson model by means of information theory. *Physica A* **2009**, *388*, 4075–4082.
14. Binder, K. Finite size scaling analysis of ising model block distribution functions. *Z. Phys. B* **1981**, *119*, 119–140.
15. Vogel, E.E.; Saravia, G.; Cortez, L.V. Data compressor designed to improve recognition of magnetic phases. *Physica A* **2012**, *391*, 1591–1601.
16. Cortez, L.V.; Saravia, G., Vogel, E.E. Phase diagram and reentrance for the 3D Edwards-Anderson model using information theory. *J. Magn. Magn. Mater.* **2014**, *372*, 173–180.
17. Vogel, E.E.; Saravia, G. Information theory applied to econophysics: stock market behaviors. *Eur. Phys. J. B* **2014**, *2014*, 4103.
18. Vogel, E.E.; Saravia, G; Astete, J.; Diaz, J.; Riadi, F. Information theory as a tool to improve individual pensions: The Chilean case. *Physica A* **424**, *2015*, 372–382.
19. Contreras, D.J.; Vogel, E.E.; Saravia, G.; Stockins B. Derivation of a measure of systolic blood pressure mutability: a novel information theory-based metric from ambulatory blood pressure tests. *J. Amer. Soc. Hypertension* **10**, *2016*, 217-223.

340 20. Vogel, E.E.; Saravia, G; Pasten, D.; Munoz, V. Time-series analysis of earthquake sequences by means of
341 information recognizer. *Tectonophysics* **712**, *2017*, 723–728.
342 21. Vogel, E.E.; Saravia, G; Ramirez-Pastor, A.J. Phase diagrams in a system of long rods on two-dimensional
343 lattices by means of information theory. *Phys. Rev. E* **96**, *2017*, 062133.
344 22. Vogel, E.E.; Saravia, G; Kobe, S.; Schumann, R.; Schuster, R. A novel method to optimize electricity generation
345 from wind energy. *Renewable Energy* **126**, *2018*, 724–735.
346 23. Binder, K. Applications of Monte Carlo methods to statistical physics. *Rep. Prog. Phys.* **1997**, *60*, 487–559.
347 24. Seung Ki Baek, Petter Minnhagen and Beom Jun Kim, True and quasi-long-range order in the generalized
348 q-state clock model *Phys. Rev. E* **2009**, 80, 060101 R.